

Title: Resolving spin, valley, and moiré quasi-angular momentum of interlayer excitons in WSe₂/WS₂ heterostructure

Authors: Chenhao Jin^{1†}, Emma C. Regan^{1,2†}, Danqing Wang^{1,2†}, M. Iqbal Bakti Utama^{1,3}, Chan-Shan Yang¹, Jeffrey Cain¹, Ying Qin⁴, Yuxia Shen⁴, Zhiren Zheng¹, Kenji Watanabe⁵, Takashi Taniguchi⁵, Sefaattin Tongay⁴, Alex Zettl¹, Feng Wang^{1,6,7*}

Affiliations:

¹ Department of Physics, University of California at Berkeley, Berkeley, California 94720, United States.

² Graduate Group in Applied Science and Technology, University of California at Berkeley, Berkeley, California 94720, United States.

³ Department of Materials Science and Engineering, University of California at Berkeley, Berkeley, California 94720, United States.

⁴ School for Engineering of Matter, Transport and Energy, Arizona State University, Tempe, Arizona 85287, United States.

⁵ National Institute for Materials Science, 1-1 Namiki, Tsukuba, 305-0044, Japan.

⁶ Material Science Division, Lawrence Berkeley National Laboratory, Berkeley, California 94720, United States.

⁷ Kavli Energy NanoSciences Institute at University of California Berkeley and Lawrence Berkeley National Laboratory, Berkeley, California 94720, United States.

† These authors contributed equally to this work

* Correspondence to: fengwang76@berkeley.edu

One Sentence Summary:

We observe multiple interlayer exciton states coexisting in a WSe₂/WS₂ heterostructure with distinct optical selection rules, which we unambiguously attribute to a moiré superlattice effect through novel optical spectroscopy.

Abstract: Moiré superlattices provide a powerful way to engineer properties of electrons and excitons in two-dimensional van der Waals heterostructures. The moiré effect can be especially strong for interlayer excitons, where electrons and holes reside in different layers and can be addressed separately. For example, it was recently proposed that the moiré superlattice potential not only localizes interlayer exciton states at different superlattice positions, but also hosts an emerging moiré quasi-angular momentum (QAM) that periodically switches the optical selection rules for interlayer excitons at different moiré sites. Here we report the observation of multiple interlayer exciton states coexisting in a WSe₂/WS₂ moiré superlattice and unambiguously determine their spin, valley, and moiré QAM through novel resonant optical pump-probe spectroscopy and photoluminescence excitation spectroscopy. We demonstrate that interlayer excitons localized at different moiré sites can exhibit opposite optical selection rules due to the spatially-varying moiré QAM. Our observation reveals new opportunities to engineer interlayer exciton states and valley physics with moiré superlattices for optoelectronic and valleytronic applications.

Main Text:

Moiré superlattices between atomically thin materials can dramatically change the properties of electrons and excitons by introducing a new length and energy scale. Artificially stacked moiré superlattices have enabled a variety of intriguing phenomena that are not available in natural systems, such as tunable Mott insulators and unconventional superconductivity (1-12). Interlayer excitons in van der Waals heterostructures have recently attracted much research interest due to their large binding energy and long lifetime (13, 14). An interlayer exciton is composed of an electron and a hole that are separated in neighboring layers, so its properties can depend strongly on the layer configurations and external fields. For example, it was recently predicted that moiré superlattices, where the interlayer atom registry changes periodically over space, can host arrays of localized interlayer exciton states with distinct valley selection rules (15, 16). The moiré degree of freedom for interlayer excitons, therefore, offers exciting opportunities towards realizing novel quantum emitter sources and exotic quantum phases like exciton Dirac and Weyl nodes (15, 16).

Direct experimental observation of the interlayer moiré excitons with registration-dependent valley selection rules, however, has been challenging. Photoluminescence (PL) has been widely used to study the interlayer excitons (17-22), but its interpretation is complicated because the PL intensity depends on both the optical transition oscillator strength and the lifetime of the emitting state. As a result, high energy interlayer exciton states cannot be conveniently probed due to their short lifetimes. In addition, it is difficult to determine the spin and momentum configuration of the emitting exciton states, or to separate different contributions to their optical selection rules. On the other hand, optical absorption measurements of interlayer exciton states are hindered by their small oscillator strength (23). Here we overcome these difficulties by probing zero-

twisting-angle WSe₂/WS₂ heterostructures with two background-free techniques: photoluminescence excitation (PLE) and resonant pump-probe spectroscopy. This combination not only allows for extremely sensitive measurements of weak absorption features associated with interlayer moiré excitons, but also unambiguously determines the nature of the interlayer excitons, including their relative oscillator strength and the spin-valley configuration of the constituent electrons and holes. We establish that interlayer excitons with the same spin-valley configuration can have opposite circular selection rules, which is attributed to the different moiré quasi-angular momentum (QAM) associated with different interlayer lattice registrations. We further show that an opposite-spin exciton state, which was originally forbidden with no valley selectivity, can gain a well-defined circular helicity in the moiré superlattice.

Figure 1, A and B show a schematic and an optical microscope image of a representative near-zero twist angle WSe₂/WS₂ heterostructure (see methods and ref. (24) for device fabrication details). Fig. 1C shows the reflection contrast of the heterostructure in the range of 1.6 to 2.4 eV. Three prominent absorption peaks are observed around the WSe₂ A exciton energy of 1.7 eV. This is a characteristic behavior of the intralayer moiré exciton, which is split into multiple peaks by a strong moiré superlattice potential (24, 25). The moiré superlattice effects on interlayer excitons are expected to be even stronger: the interlayer excitons are predicted to localize at different potential minima within the moiré superlattice, labelled as point A and B in Fig. 1D (15, 16). Consequently, four low energy interlayer moiré exciton states can exist in the K valley, i.e. the same-spin and opposite-spin states centering at A and B points within the moiré superlattice, respectively. These four states are illustrated in Fig. 1D, and their time-reversal pairs create another set of 4 states in the K' valley (not shown).

However, photoluminescence (PL) spectrum of the WS₂/WSe₂ heterostructure shows a single prominent emission peak at 1.43 eV (Fig. 1D), corresponding to only one interlayer exciton state. Although the PL emission spectrum is extremely sensitive, it is not sufficient to probe different interlayer exciton states or the nature of the interlayer excitons: The lowest energy exciton state, which has the longest population lifetime, can dominate the PL emission irrespective of its spin or valley characteristics.

We use helicity-resolved photoluminescence excitation (PLE) spectroscopy to probe higher energy interlayer moiré exciton states in the WS₂/WSe₂ heterostructure. We monitor both the σ^+ - and σ^- -polarized PL emission intensity at 1.43 eV while continuously varying the energy of the excitation photons with σ^+ helicity. Figure 2A and 2B show the PLE spectra: the energy of σ^+ excitation light is scanned over the WSe₂ intralayer exciton range (1.65 to 1.92 eV, Fig. 2A) and interlayer exciton range (1.45 to 1.55 eV, Fig. 2B). The helicity contrast for intralayer and interlayer excitation ranges are displayed in Fig. 2C and 2D, respectively. The PL emission intensity is proportional to the absorbed photon number and provides a sensitive measurement of the absorption oscillator strength. Strongly-enhanced PL signal is observed when the excitation light is on resonance with the intralayer exciton resonances (Fig. 2A). We also observe well-defined absorption resonances in the interlayer exciton range at 1.46 (green shaded region in Fig. 2B) and 1.51 eV (yellow shaded region). These resonances correspond to two new interlayer moiré exciton states, and their oscillator strengths are more than 100 times smaller than the intralayer exciton transitions. Such weak interlayer exciton transitions are extremely difficult to measure in a direct absorption measurement but are readily observable in the background-free PLE spectroscopy. Furthermore, we observe distinctively different circular helicity behaviors between the intralayer and interlayer excitons: The circular helicity has a large and near-constant

value of ~ 0.5 over the whole intralayer exciton range (Fig. 2C), but changes dramatically and can have opposite signs for different interlayer exciton resonances (Fig. 2D, see supplementary).

To resolve the spin and valley properties and to understand the unusual optical selection rules of different interlayer moiré exciton states, we employ resonant pump-probe spectroscopy. As illustrated in Fig. 3A, we resonantly excite an interlayer exciton transition with circularly polarized pump light, and then probe the spin-valley state of the constituent holes in the WSe₂ layer by monitoring the induced absorption changes in the WSe₂ intralayer exciton transitions. This method takes advantage of the fact that the intralayer exciton optical selection rules have already been well established in previous studies (26-28), and they are independent of the relative registration of the two layers (15, 16). Further, the interlayer exciton oscillator strength can be obtained from the signal magnitude of the resonant interlayer-exciton-pump and intralayer-exciton-probe measurements.

Figure 3B shows the pump-induced circular dichroic signal with probe energy fixed at 1.67 eV (near a WSe₂ intralayer exciton feature) and pump energy swept from 1.38 eV to 1.54 eV. Strong pump-probe signals with opposite signs are observed at 1.46 and 1.51 eV (green and yellow shaded regions, respectively). This result reaffirms the PLE observation of two interlayer exciton states at 1.46 and 1.51 eV with different helicity. Interestingly, no clear absorption resonance is observed at the energy of the PL emission peak (purple shaded region around 1.43 eV). This indicates that the interlayer exciton state that dominates the emission process of the system has small absorption oscillator strength. We label it as a “weakly-absorbing” interlayer exciton state, in contrast to the “strongly-absorbing” states at 1.46 and 1.51 eV.

We further resonantly excite the strongly-absorbing interlayer exciton states using σ^+ pump light and measure the induced circular dichroic spectra in the WSe₂ intralayer exciton range (Fig. 3, C

and D). These results can be compared to the pump-probe responses when directly exciting the intralayer exciton at 1.94 eV (Fig. 3E), where the optical selection rule is well established and not affected by the moiré superlattice (15, 16). All three spectra profiles are similar and display prominent resonance features around probe energy of 1.68 eV and 1.73 eV, corresponding to the peak I and II of intralayer moiré exciton states in WSe₂, respectively (Ref. (24)). This is expected because the pump-probe signals originate from the response of intralayer excitons to valley-polarized holes in WSe₂. The sign of the signals, however, are different for the two interlayer exciton states. Pumping at 1.51 eV gives a signal of the same sign as pumping the intralayer exciton. This interlayer exciton state therefore has the same optical selection rule as the intralayer exciton, i.e. σ^+ light selectively creates holes in the K valley of WSe₂ (inset of Fig. 3D and Fig. 3E). In contrast, pumping at 1.46 eV gives an opposite sign, indicating that σ^+ light selectively create holes in the K' valley (inset of Fig. 3C). In other words, the 1.51 eV and 1.46 eV interlayer exciton states in the K valley will couple more efficiently to σ^+ and σ^- light, and therefore have a total quasi-angular momentum (QAM) of +1 and -1, respectively (see supplementary).

Based on the spin-valley state of the hole in the WSe₂ layer and the interlayer exciton oscillator strength, we can infer the spin-valley configuration of the electron within the interlayer exciton and determine the emerging moiré quasi-angular momentum, as shown in Table 1. The electron and hole must be in the same valley and of the same spin for the “bright” 1.46 and 1.51 eV interlayer exciton states to exhibit relatively strong oscillator strengths. Therefore, we can assign a spin contribution of 0 and valley contribution of +1 from the constituent electron and hole to the QAM of K-valley interlayer exciton (see supplementary). The rest of the contribution to the QAM arises from the local interlayer atomic registration in the moiré superlattice. Consequently,

we determine a moiré QAM of -2 for the 1.46 eV interlayer exciton and zero for the 1.51 eV interlayer exciton. They correspond to the second (moiré position B) and fourth state (moiré position A) illustrated in Fig. 1D, respectively.

The lowest energy interlayer exciton state at 1.43 eV has weak oscillator strength, and we attribute it to an interlayer exciton with opposite electron and hole spin based on the electronic bands of the heterostructure (Fig. 1D). This arises naturally because the spin-orbital coupling has opposite sign in the conduction and valence bands for W-based transition metal dichalcogenide materials (29, 30). This opposite spin state is not completely dark, since spin is no longer a good quantum number in systems with strong spin-orbital coupling (31, 32). The energy separation between the opposite- and same-spin interlayer excitons (state 1 and 2) is ~ 30 meV, which is also consistent with the known conduction band spin splitting in WS₂ layers (29, 30). Previously, an intralayer opposite-spin exciton has been observed in the PL emission of monolayer WSe₂ without a magnetic field (33, 34); however, it shows no circular valley selection, as its QAM only comes from spin-valley contribution and is 0 (Ref. (31, 32)). In contrast, emission from the 1.43 eV interlayer exciton state shows a large σ^+ circular helicity when we excite intralayer excitons with σ^+ -polarized light (Fig. 2B). It indicates that the lowest energy K-valley interlayer exciton has a total QAM of +1 (state 1 in Fig. 1D). This again highlights the important role of moiré superlattice, which introduces an additional QAM of +1 (or equivalently, -2, due to the three-fold rotation symmetry in the system) and a well-defined circular selection rule to the lowest-energy opposite-spin state. The other opposite-spin state, i.e. state 3, is not observed in our study, presumably due to its very small oscillator strength.

Combining the ability to engineer spin-valley selection rules using the novel moiré degree of freedom, the coexistence of multiple moiré states with distinctively different optical properties,

and the tunability from layer configuration and external fields, interlayer excitons in WSe_2/WS_2 moiré superlattice provides a versatile platform to exciting new exciton and valley physics.

References

1. B. Hunt *et al.*, *Science* **340**, 1427 (2013).
2. L. A. Ponomarenko *et al.*, *Nature* **497**, 594 (2013).
3. C. R. Dean *et al.*, *Nature* **497**, 598 (2013).
4. Y. Cao *et al.*, *Nature* **556**, 43 (2018).
5. Y. Cao *et al.*, *Nature* **556**, 80 (2018).
6. G. Chen *et al.*, *Arxiv*, 1803.01985 (2018).
7. Z. W. Shi *et al.*, *Nat Phys* **10**, 743 (2014).
8. E. M. Spanton *et al.*, *Science* **360**, 62 (2018).
9. J. R. Wallbank, A. A. Patel, M. Mucha-Kruczynski, A. K. Geim, V. I. Falko, *Phys Rev B* **87**, 245408 (2013).
10. J. C. W. Song, P. Samutpraphoot, L. S. Levitov, *P Natl Acad Sci USA* **112**, 10879 (2015).
11. R. V. Gorbachev *et al.*, *Science* **346**, 448 (2014).
12. M. Lee *et al.*, *Science* **353**, 1526 (2016).
13. P. Rivera *et al.*, *Nature Communications* **6**, 6242 (2015).
14. S. Latini, K. T. Winther, T. Olsen, K. S. Thygesen, *Nano Letters* **17**, 938 (2017).
15. H. Y. Yu, G. B. Liu, J. J. Tang, X. D. Xu, W. Yao, *Sci Adv* **3**, e1701696 (2017).
16. F. C. Wu, T. Lovorn, A. H. MacDonald, *Phys Rev B* **97**, 035306 (2018).
17. W. T. Hsu *et al.*, *Nature Communications* **9**, 1356 (2018).
18. A. T. Hanbicki *et al.*, *ACS Nano* **12**, 4719 (2018).
19. K. Tran *et al.*, *Arxiv*, 1807.03771 (2018).
20. K. Seyler *et al.*, *Arxiv*, 1809.04562 (2018).
21. A. Ciarrocchi *et al.*, *Nature Photonics*, <https://doi.org/10.1038/s41566> (2018).
22. L. Zhang *et al.*, *Arxiv*, 1901.00200 (2019).
23. J. S. Ross *et al.*, *Nano Letters* **17**, 638 (2017).
24. C. H. Jin *et al.*, *Arxiv*, 1812.09815 (2018).
25. F. C. Wu, T. Lovorn, A. H. MacDonald, *Phys Rev Lett* **118**, 147401 (2017).
26. T. Cao *et al.*, *Nature Communications* **3**, 887 (2012).
27. K. F. Mak, K. He, J. Shan, T. F. Heinz, *Nature Nanotechnology* **7**, 494 (2012).
28. D. Xiao, G.-B. Liu, W. Feng, X. Xu, W. Yao, *Phys Rev Lett* **108**, 196802 (2012).
29. K. Andor *et al.*, *2D Materials* **2**, 022001 (2015).
30. X.-X. Zhang, Y. You, S. Y. F. Zhao, T. F. Heinz, *Phys Rev Lett* **115**, 257403 (2015).
31. G. Wang *et al.*, *Phys Rev Lett* **119**, 047401 (2017).
32. J. P. Echeverry, B. Urbaszek, T. Amand, X. Marie, I. C. Gerber, *Phys Rev B* **93**, 121107 (2016).
33. S. Y. Chen, T. Goldstein, T. Taniguchi, K. Watanabe, J. Yan, *Nature Communications* **9**, 3717 (2018).
34. Z. P. Li *et al.*, *Nature Communications* **9**, 3719 (2018).
35. L. Wang *et al.*, *Science* **342**, 614 (2013).
36. J. Kim *et al.*, *Sci Adv* **3**, e1700518 (2017).
37. J. Kim *et al.*, *Science* **346**, 1205-1208, (2014).
38. Z. L. Ye *et al.*, *Nature* **513**, 214-218, (2014).
39. A. Chernikov *et al.*, *Phys Rev Lett* **113**, 076802(2014).

Acknowledgements:

Funding: This work was supported primarily by the Director, Office of Science, Office of Basic Energy Sciences, Materials Sciences and Engineering Division of the U.S. Department of Energy under contract no. DE-AC02-05-CH11231 (van der Waals heterostructures program, KCWF16). PLE spectroscopy of the heterostructure is supported by the US Army Research Office under MURI award W911NF-17-1-0312. Growth of hexagonal boron nitride crystals was supported by the Elemental Strategy Initiative conducted by the MEXT, Japan and JSPS KAKENHI Grant Numbers JP15K21722. S.T. acknowledges the support from NSF DMR 1552220 NSF CAREER award for the growth of WS₂ and WSe₂ crystals. E.C.R acknowledges support from the Department of Defense (DoD) through the National Defense Science & Engineering Graduate Fellowship (NDSEG) Program.

Author contributions: C.J., E.C.R., and D.W. contributed equally to this work. F.W. and C.J. conceived the research. C.J., E.C.R. and D.W. carried out optical measurements. C.J., F.W. and E.C.R. performed theoretical analysis. E.C.R., D.W., M.I.B.U. and Z.Z. fabricated van der Waals heterostructures. Y.Q., S.Y., S.T., J.C., and A.Z. grew WSe₂ and WS₂ crystals. K.W. and T.T. grew hBN crystals. All authors discussed the results and wrote the manuscript.

Competing interests: The authors declare no competing interests.

Data and materials availability: The data that support the findings of this study are available from the corresponding author upon reasonable request.

Supplementary Materials:

Materials and Methods

Figures S1-S2

References 35-39

Figures:

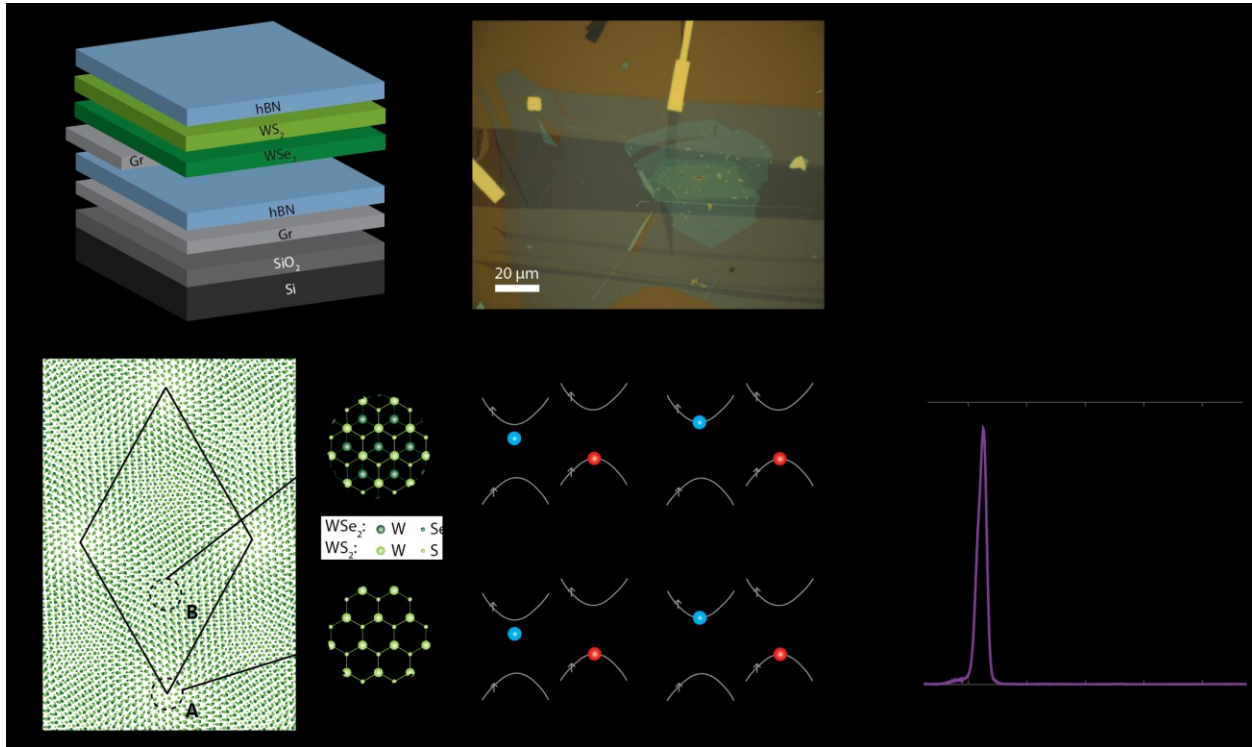


Fig. 1 | Interlayer moiré excitons in near-zero twist angle WSe₂/WS₂ heterostructure. (A and B) Side-view illustration (A) and optical microscope image (B) of a representative near-zero twist angle heterostructure. (C) Reflection contrast of the heterostructure shows three prominent peaks in the WSe₂ A exciton range near 1.7 eV. This is a characteristic absorption signature of the intralayer moiré exciton. (D) Illustration of the moiré superlattice in real space (left) with moiré supercell outlined in black diamond. Interlayer excitons can be trapped at two different local minima of the moiré potential, labeled as A and B points. This moiré degree of freedom, combined with different spin configurations, give rise to 4 interlayer exciton states in the K valley (state 1 to 4 in the right box). (E) Photoluminescence (PL) spectrum of the heterostructure shows only one prominent peak at 1.43 eV because PL measurements are only sensitive to the emission state and cannot probe higher energy states.

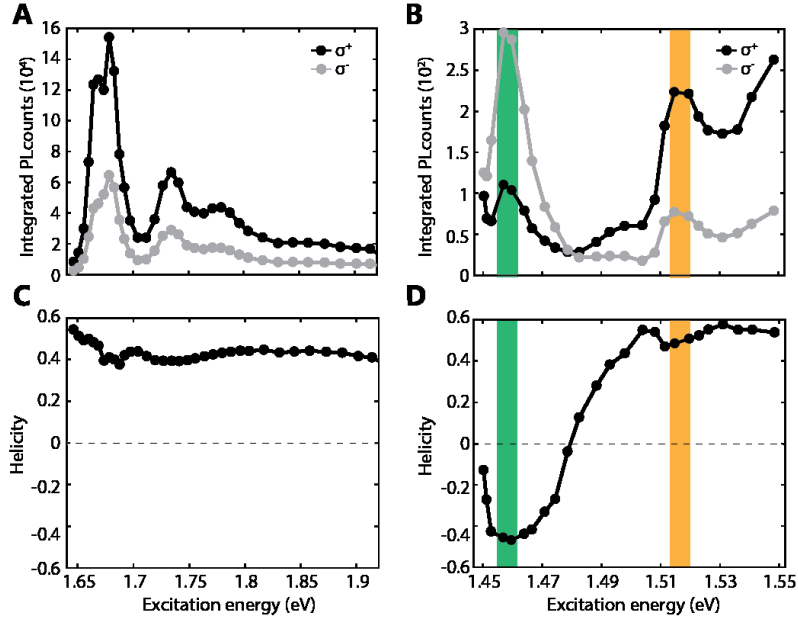


Fig. 2 | Interlayer moiré excitons probed by helicity-resolved photoluminescence excitation (PLE) spectroscopy. (A and B) PLE spectra of a representative device measured by monitoring the σ^+ (black) and σ^- (grey) emission intensity of the 1.43 eV emission peak. The energy of σ^+ excitation light is scanned over intralayer exciton (A) and interlayer exciton (B) range. The emission intensity is strongly enhanced when excitation light is in resonance with all intralayer exciton resonances (A) and two additional resonance peaks in the interlayer exciton range (B), suggesting the existence of two new interlayer moiré exciton states at 1.46 (green shaded area) and 1.51 eV (yellow shaded area), respectively. (C) PL circular helicity shows a near-constant positive value of ~ 0.5 with intralayer exciton excitation. (D) PL emission shows circular helicity of ~ 0.5 and ~ -0.5 when exciting the 1.46 and 1.51 eV interlayer exciton states, revealing their unusual optical selection rules. All measurements are done at 10 Kelvin.

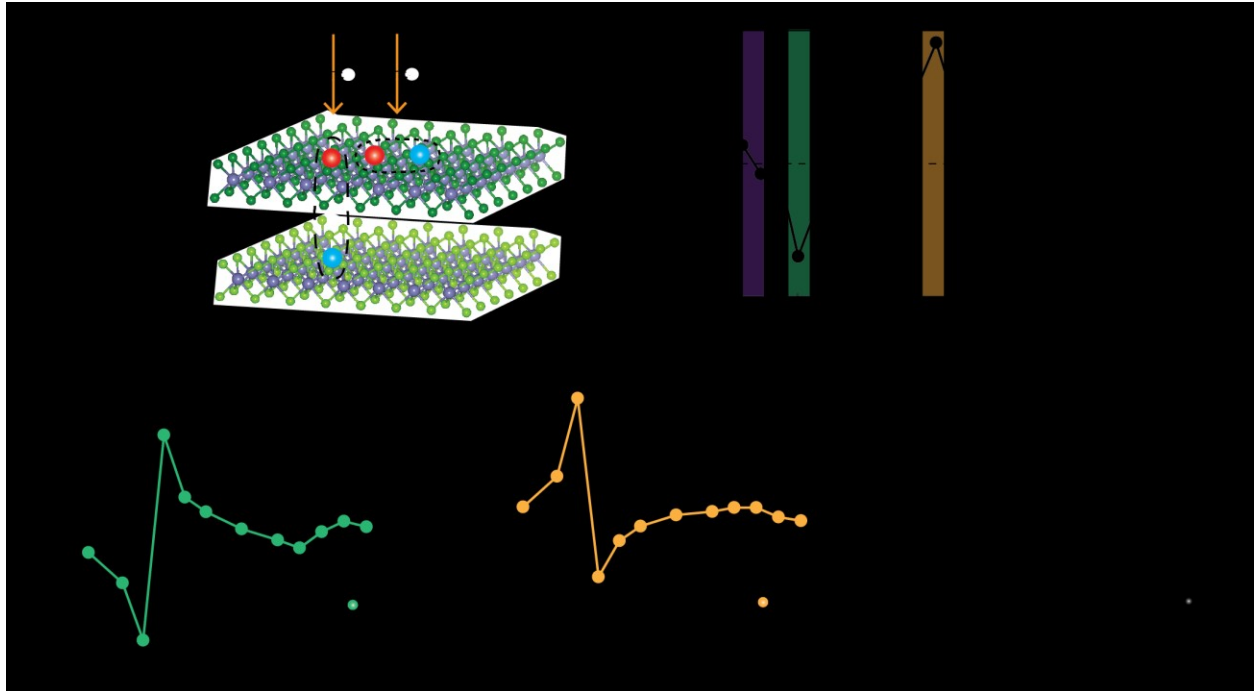


Fig. 3 | Interlayer moiré excitons probed by resonant pump-probe spectroscopy. (A) Illustration of the pump-probe experimental design. σ^+ pump light in resonance with an interlayer exciton state directly creates valley-polarized holes in WSe₂, which can then be probed by the induced circular dichroic signal at the WSe₂ intralayer exciton energy. (B) Pump-induced circular dichroic signal with probe energy fixed at 1.67 eV and pump energy swept from 1.38 eV to 1.54 eV. The two prominent resonances with opposite sign at 1.46 (green shaded region) and 1.51 eV (yellow shaded region) reaffirms the two interlayer moiré exciton states observed in PLE measurement. The 1.43 eV state, on the other hand, shows no clear resonance (purple shaded region), indicating its weakly-absorbing nature. (C to E) Pump-induced circular dichroic spectra with pump energy in resonance with the 1.46 eV state (C), 1.51 eV state (D), and intralayer exciton at 1.94 eV (E). The circular dichroic spectra when pumping the 1.51 eV interlayer exciton state gives the same sign as when pumping the intralayer exciton; therefore in both cases σ^+ pump create holes in the K valley of WSe₂ (insets of (D) and (E)). In contrast, an opposite sign is observed when pumping the 1.46 eV state, indicating that σ^+ light selectively create holes in the K' valley (insets of (C)). All measurements are done at 10 Kelvin.

State	Energy (eV)	Oscillator Strength	Total QAM	Hole	Electron	Spin QAM	Valley QAM	Moiré QAM	Moiré Position
1	1.43	Weak	+1 = -2	K ↑	K ↓	-1	+1	-2	B
2	1.46	Strong	-1	K ↑	K ↑	0	+1	-2	B
3		Not observed	0	K ↑	K ↓	-1	+1	0	A
4	1.51	Strong	+1	K ↑	K ↑	0	+1	0	A
5	1.43	Weak	-1 = +2	K' ↓	K' ↑	1	-1	+2	B
6	1.46	Strong	+1	K' ↓	K' ↓	0	-1	+2	B
7		Not observed	0	K' ↓	K' ↑	1	-1	0	A
8	1.51	Strong	-1	K' ↓	K' ↓	0	-1	0	A

Table 1: Nature of different interlayer moiré exciton states and the spin, valley and moiré contributions to their optical selection rule